Vol. 628: 1–16, 2019
https://doi.org/10.3354/meps13143

MARINE ECOLOGY PROGRESS SERIES
Mar Ecol Prog Ser

Published October 10

FEATURE ARTICLE

An invasive macroalga alters ecosystem metabolism and hydrodynamics on a tidal flat

Martin P. Volaric*, Peter Berg, Matthew A. Reidenbach

Department of Environmental Sciences, University of Virginia, Charlottesville, Virginia 22904, USA

ABSTRACT: Invasive macroalgae represent a growing global concern, yet there has been little research detailing their effects on native ecosystem metabolism and flow hydrodynamics. In this *in situ* study, we made aquatic eddy covariance oxygen flux and profiling acoustic Doppler velocimetry measurements over high and low density sites within an invasive *Gracilaria vermiculophylla* (also referred to as *Agarophyton vermiculophyllum*) macroalgal mat located on a tidal flat along the Virginia (USA) coast. Mean ± SE (n) submerged dark and light oxygen flux over the high density site were −178 ± 9 (144) and 139 ± 26 (104) mmol m^{-2} d^{-1}, respectively, vs. −71 ± 7 (45) and 32 ± 15 (48) mmol m^{-2} d^{-1} over the low density site. The high density site was highly productive, with gross primary production of 169 ± 12 mmol m^{-2} d^{-1} (mean ± SE), yet maintained overall metabolic balance, as net ecosystem metabolism was −22 ± 39 mmol m^{-2} d^{-1}. Close agreement with literature values for air-exposed flux measurements suggests that our results are good first-order approximations of true daily values, demonstrating that this invasion has significantly enhanced tidal flat productivity. Flow and turbulence were significantly attenuated by *Gracilaria*, resulting in decreased bed shear stress within the algal canopy, likely stabilizing tidal flat sediments and inhibiting mass transport at the sediment–water interface. Turbulence above the canopy was enhanced, but there was no increase in downward momentum transfer. These changes to the hydrodynamic environment decrease the risk of detachment and subsequent advective loss of algae, suggesting a positive feedback that facilitates algal invasion.

KEY WORDS: Invasive seaweeds · Macroalgae · *Gracilaria vermiculophylla* · Oxygen flux · Aquatic eddy covariance · *Agarophyton vermiculophyllum* · Productivity

*Corresponding author: mpv3a@virginia.edu

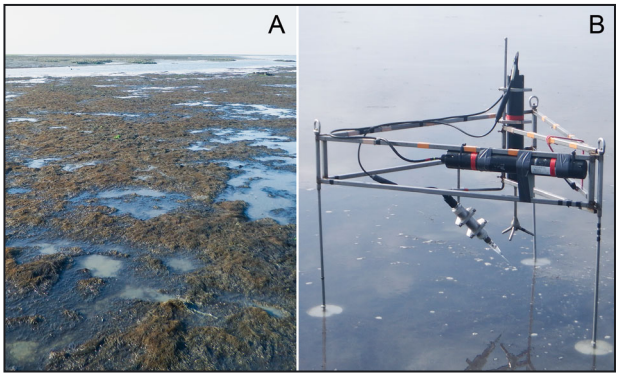

Ecosystem metabolism of (A) an invasive *Gracilaria vermiculophylla* macroalgal mat was measured *in situ* using (B) the aquatic eddy covariance technique.

Photos: Martin P. Volaric

1. INTRODUCTION

Invasive macroalgae have become a major area of research due to the wide range of impacts they impart on native systems. Their potential effects have been viewed as both positive (e.g. enhanced macrofaunal biomass and diversity; Lyons et al. 2014, Ramus et al. 2017), and negative (increased hypoxia, loss of native macrophytes; Inderjit et al. 2006, Schaffelke et al. 2006, Lyons et al. 2014). Therefore, when a new algal invader is identified within a marine system, it is imperative that a careful analysis of its impact on ecosystem function be conducted so that resource managers can make informed decisions (Thresher & Kuris 2004).

Although nonnative macroalgae can drastically alter local ecosystem metabolism, relatively few studies have detailed the magnitude of these effects (Lyons et al. 2014), with previous invasions having been shown to both increase (Dumay et al. 2002) and decrease (Salvaterra et al. 2013) ecosystem productivity.

Publisher: Inter-Research · www.int-res.com

One invasive macroalga that has increasingly been identified within coastal waters along the USA and Europe is the red seaweed *Gracilaria vermiculophylla* (Thomsen et al. 2005, Gulbransen et al. 2012, Krueger-Hadfield et al. 2017, 2018), also referred to as *Agarophyton vermiculophyllum* (Gurgel et al. 2018), and hereafter referred to as *Gracilaria*. Originally native to Japan (Ohmi 1956), this alga is believed to have been spread through oyster aquaculture (Gulbransen et al. 2012, Krueger-Hadfield et al. 2017). Along the US mid-Atlantic coast, *Gracilaria* often colonizes previously bare tidal flats, where its invasion is facilitated by burrowing polychaetes (decorator worms *Diopatra cuprea*), which attach algae to their tubes, resulting in large intertidal mats (Thomsen et al. 2006). Drift algae such as *Gracilaria* can affect tidal flat function in numerous ways, including by providing structure and a food source to macrofauna (Nyberg et al. 2009, Byers et al. 2012, Davoult et al. 2017), increasing hypoxia near the sediment surface (Valiela et al. 1997), and decreasing the settlement success of larval sessile organisms such as oysters (Thomsen & McGlathery 2006).

Given the addition of a large phototrophic biomass, the establishment of *Gracilaria* appears likely to increase tidal flat primary production. However, previous work has demonstrated mixed results (Tyler & McGlathery 2006, Cacabelos et al. 2012, Davoult et al. 2017), and consequently, researchers have recently argued that there is a need for more precise measurements of *Gracilaria*'s impact on ecosystem productivity (Byers & Sotka 2019, Sotka & Byers 2019, Thomsen et al. 2019). Measurements of benthic oxygen flux address this research gap, as they are a proxy for the primary production, heterotrophic activity, and integrated carbon metabolism of benthic systems (Glud 2008). To date, few studies have focused on *Gracilaria* metabolism (Cacabelos et al. 2012, Davoult et al. 2017), and to our knowledge, only 1 study has measured oxygen flux during submerged conditions (Cacabelos et al. 2012), using *ex situ* core incubations.

Aquatic eddy covariance (AEC) is a relatively new alternative technique for measuring benthic oxygen fluxes in aquatic systems (Berg et al. 2003), representing an adaptation of a long-used method for quantifying atmospheric scalar fluxes (e.g. Priestly & Swinbank 1947). Unlike core incubations, AEC measurements are conducted *in situ* and are non-invasive (Lorrai et al. 2010), have a high temporal resolution (Rheuban & Berg 2013), and integrate over a large benthic surface area (Berg et al. 2007). With these advantages, AEC measurements are able to quantify benthic oxygen fluxes under natural conditions, and have been used to study the oxygen metabolism of several heavily vegetated benthic ecosystems, including seagrass meadows (Rheuban et al. 2014a, Berg et al. 2019), maerl beds (Attard et al. 2015), and *Fucus vesiculosus* canopies (Attard et al. 2019).

In addition to its effects on ecosystem productivity, *Gracilaria* is also likely to alter the flow and turbulence of invaded tidal flats. Macroalgal mats can impact hydrodynamics throughout the water column, as flow within algal canopies typically has lower horizontal flow speed and Reynolds stress (Finnigan 2000, Hurd 2000), while flow above canopies is characterized by increased friction velocity and turbulence (Venier et al. 2012). These effects dampen bed shear stress, which enhances sediment stability and inhibits mass transport (Venier et al. 2012, Stocking et al. 2016). However, the magnitude of these impacts can vary greatly based on algal type and density (Hurd 2000), and the overall impact of *Gracilaria* on tidal flat hydrodynamics and sediment transport is not well understood. A previous study using gypsum dissolution blocks demonstrated a significant effect of *Gracilaria* biomass on flow attenuation, but not on sediment accumulation (Ramus et al. 2017), while past laboratory studies have shown that relatively moderate flow velocities (11–13 cm s^{-1}) can transport unattached clumps of *Gracilaria* as bedload, disturbing sediments and increasing resuspension (Canal-Vergés et al. 2010, Lawson et al. 2012). Inhibited mass transport at the sediment–water interface stemming from flow attenuation can have a profound impact on biogeochemical cycling in coastal sediments (Boudreau & Jørgensen 2001) and on benthic production (Lawson et al. 2007). Therefore, as with ecosystem productivity, there is a need to quantify how the addition of *Gracilaria* to tidal flats can alter these key ecosystem processes.

In this study, we made AEC oxygen flux and profiling flow and turbulence measurements over low and high algal density sites within a *Gracilaria* mat located on a tidal flat on the coast of Virginia (USA). Previous AEC measurements were performed over this same tidal flat 2 yr prior to our sampling when almost no macroalgae were present (Volaric et al. 2018), and served as a baseline comparison for how *Gracilaria* has impacted the metabolism of the flat. Given past results, we hypothesized that (1) there would be a significant enhancement of oxygen metabolism — both production and consumption — between bare, low density, and high density sites, and (2) flow and turbulence would be significantly dampened by the *Gracilaria* canopy, reducing bed shear stress.

2. MATERIALS AND METHODS

2.1. Study site

Field research was conducted June 2017 over an intertidal *Gracilaria* mat situated on a tidal flat within the Hillcrest Oyster Sanctuary, which itself is contained within the Virginia Coast Reserve (VCR), part of the US National Science Foundation's Long-Term Ecological Research network. This tidal flat was covered with a variable density of macroalgae, composed primarily of clumps of *Gracilaria* attached to *Diopatra cuprea* worm tubes along with a small quantity of unattached *Ulva* sp. Depth at high tide was approximately 1–1.5 m. Two sites along this flat were chosen for comparative analysis: one with a high density of algae (GPS: 37.2833° N, 75.9047° W) and one with a low density (37.2840° N, 75.9049° W; Fig. 1A,B). These sites were approximately 100 m from one another and had mean algal coverages 61.2 ± 11% and 25.2 ± 5.1% (mean ± SE, n = 8), respectively (Table 1). Algal coverage was determined using 0.5 m × 0.5 m quadrats placed randomly within the approximate 'footprint' of the AEC systems, defined as the smallest benthic surface area that contributes 90% of the flux signal (Berg et al. 2007). The footprint was previously estimated for this tidal flat as ~50 m long on either side of the AEC system, depending on flow direction (Volaric et al. 2018). Each quadrat was photographed and analyzed for areal density using Adobe Photoshop©. *Gracilaria* biomass within the VCR peaks in the early summer (Thomsen et al. 2006), so this sampling period occurred during peak algal coverage.

At both sites, the sediment organic matter, grain size, and chlorophyll *a* (chl *a*) content were measured. Sediment organic matter was determined as percent mass loss on ignition (6 h at 500°C). Sediment grain size was measured using a laser diffraction particle size analyzer (Beckman Coulter LS I3 320). Sediment samples were sieved at 1 mm, treated with hydrogen peroxide to remove particulate organic matter, and categorized by D_{84}, which is the diameter of the 84th percentile of particle size. Benthic chl *a*

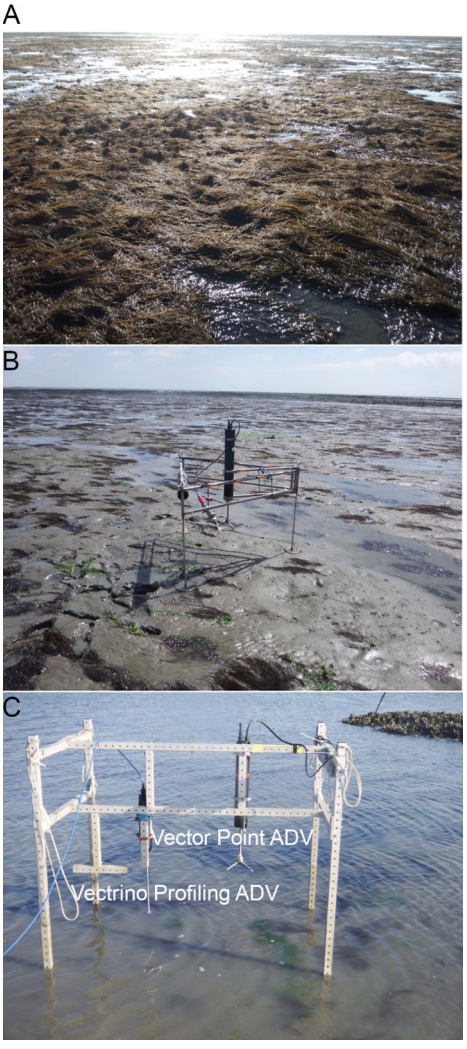

Fig. 1. Study site in *Gracilaria* mat situated on a tidal flat within the Virginia Coast Reserve, USA. Aquatic eddy covariance (AEC) and flow hydrodynamic measurements were made over both (A) high and (B) low (shown with AEC system) density sites in June 2017. (C) Horizontal velocity and turbulence profiles were determined using a Nortek AS Vectrino© profiling acoustic Doppler velocimeter (ADV), with an additional Vector point ADV placed well above the canopy (35 cm) in order to determine free stream conditions. All images here show emergent conditions, but this study only includes measurements made when these sites were submerged

Table 1. Site characteristics of both sampling locations, including: sediment organic matter content (OM), chl *a* content, grain size (D_{84}), algal cover of 2 dominant algae (*Gracilaria vermiculophylla* and *Ulva* sp.), and mean flow speed (u) during light and dark conditions. Values of u are 15 min averages of data taken concurrently with aquatic eddy covariance data collection. All values represent mean ± SE (n)

Site	OM (%)	Chl *a* (mg m^{-2})	D_{84} (µm)	*Gracilaria* (%)	*Ulva* (%)	u_{LIGHT} (cm s^{-1})	u_{DARK} (cm s^{-1})
Low density	1.75 ± 0.07 (8)	39.5 ± 2.7 (8)	181 ± 2.8 (8)	20.7 ± 4.1 (8)	4.5 ± 4.0 (8)	12 ± 0.7 (48)	9.2 ± 0.9 (45)
High density	1.32 ± 0.07 (8)	37.9 ± 3.8 (8)	181 ± 2.8 (8)	61.2 ± 11 (8)	0 ± 0 (8)	13 ± 0.6 (104)	14 ± 0.6 (144)

was determined using a methanol–acetone extraction combined with a Shimadzu UV 1800 spectrophotometer (Lorenzen 1967).

2.2. Aquatic eddy covariance

The AEC system consists of a Nortek AS Vector© acoustic Doppler velocimeter (ADV) connected to a fast-response (90% response time ≤0.4 s) Unisense AS Clark-type oxygen microelectrode (stirring sensitivity <1% according to the manufacturer) by a high-resolution custom-made picoamp amplifier (Berg & Huettel 2008). These instruments were mounted together on a stainless-steel frame, and were powered by the same external battery (Fig. 1B). The ADV has a cylindrical measurement volume approximately 14 mm in diameter and 14 mm in height, and the electrode was placed 0.5 cm from its edge so as not to interfere with data collection. The height of this measuring volume was 10 cm from the sediment surface at the low density site and 20 cm from the sediment surface at the high density site (canopy height ≈ 10 cm). These distances were chosen to balance the smoothing of heterogeneity effects (Rheuban & Berg 2013) against the desire to maximize data collection intervals at these intertidal sites.

Together, the ADV and electrode made 32 Hz measurements of the 3 velocity components (u, v, w) and oxygen concentration (C). These measurements were made over 15 min bursts consisting of a 14.5 min interval of data collection followed by a 0.5 min pause, with the ADV's internal recorder capable of storing up to 60 h of data. Two systems were used –one at the high density site and one at the low density site– in order to account for environmental fluctuations. Only data taken when both the ADV and oxygen microelectrode were submerged were analyzed, which occurred approximately 5–7 h per tidal cycle or 10–14 h d^{-1}. These data additionally contained some gaps due to sensor breakage and/or malfunction (see below). In total, nearly 90 h of high-quality AEC data were collected and used for further analysis.

Autonomous PME miniDOT© oxygen optodes were used to calibrate the concentration measured by the microelectrodes. Concurrent underwater photosynthetically active radiation (PAR) measurements were made using Odyssey loggers that were calibrated as described by Long et al. (2012). Both miniDOTs and PAR loggers were placed close to the eddy systems, and at the same depth as the ADV measurement volume.

Following extraction from the ADV, the 32 Hz AEC data were averaged down to 8 Hz in order to reduce unbiased noise (Berg et al. 2009). Total oxygen flux J_{O_2} between the benthos and the water column was calculated as:

$$\overline{J_{O_2}} = \overline{w'C'} \quad (1)$$

where w' and C' are the instantaneous fluctuations away from the mean of the vertical velocity and oxygen concentration, respectively, and the overbars indicate time averaging (Berg et al. 2003). This calculation was made using the software package 'EddyFlux' Ver 3.00 (P. Berg unpubl.). Velocity and oxygen concentration means for most (~85%) bursts were determined using a least-squares linear fit of the 8 Hz data over each 15 min interval (Lee et al. 2004, Berg et al. 2009). The remaining ~15% showed signs of large-scale non-linear fluctuations in oxygen concentration or velocity that were not attributable to turbulent eddies or tidal flow. The means for these data were determined using a 90 s running average (Lee et al. 2004, Volaric et al. 2018). Each 15 min burst was examined for sensor malfunctions as identified by data spikes, excessive signal noise, or abrupt variation from the optode oxygen signal (Lorrai et al. 2010), with any data showing signs of these anomalies removed. Small-wave activity, identified by sinusoidal velocity patterns, was observed in much of the ADV velocity data. Time-shifting AEC data under wavy conditions can result in severe measurement bias (Berg et al. 2015, Reimers et al. 2016), so no time-shift was applied to the oxygen data when calculating the flux.

Due to the intertidal nature of our sites, data could not be collected in continuous 24 h segments, and respiration (R) was defined as the mean dark flux for each site. The combined data for the high density site encompassed all hours of the day, allowing us to create a 24 h composite daily flux. Using this composite flux, we calculated both the submerged gross primary production (GPP) and submerged net ecosystem metabolism (NEM), as described by Hume et al. (2011):

$$\mathrm{GPP} = \frac{1}{24}\left(\sum \mathrm{flux}_{\mathrm{LIGHT}} + \frac{|\,\mathrm{flux}_{\mathrm{DARK}}\,|}{h_{\mathrm{DARK}}} h_{\mathrm{LIGHT}}\right) \quad (2)$$

$$\mathrm{NEM} = \frac{1}{24}\left(\sum \mathrm{flux}_{\mathrm{LIGHT}} + \mathrm{flux}_{\mathrm{DARK}}\right) \quad (3)$$

where h_{LIGHT} and h_{DARK} are the number of specific hours (e.g. 07:00–08:00 h, 08:00–09:00 h, etc.) out of 24 that were predominantly light or dark, respectively, during the study period, and $\mathrm{flux}_{\mathrm{LIGHT}}$ and $\mathrm{flux}_{\mathrm{DARK}}$ are the associated mean hourly fluxes.

At the low density site, not all hours of the day were covered by the composite flux data. For this site, we estimated hourly nighttime fluxes as the mean nighttime flux. Hourly daytime flux values were interpolated using a hyperbolic tangential photosynthesis–irradiance (P-I) relationship (Jassby & Platt 1976, Rheuban et al. 2014b) fit to daytime data:

$$\text{Flux} = P_{\max} tanh \frac{I}{I_S} - R_I \quad (4)$$

where $P_{\max}$, I_S, and R_I are fitting parameters representing the maximum photosynthetic rate, saturating light level, and respiration, respectively. For the purpose of this interpolation, I refers to the mean hourly PAR from the high density site, which was used to control for possible differences in light between the 2 sites.

2.3. Hydrodynamics

Horizontal flow speed and turbulence profiles were determined at both sites using a Nortek© Vectrino Profiler (Fig. 1C), a specialized ADV that makes high-frequency velocity measurements at 0.1 cm bins along a 3 cm vertical profile, for a total of 31 measurements per profile. Although the low and high density sites had algal coverages of 25 and 61%, respectively (Table 1), these densities were averages of coverage within the AEC measurement footprint (see Section 2.1). In order to better constrain the effect of *Gracilaria* on tidal flat hydrodynamics, the Vectrino was deployed over a particularly large, dense patch of algae at the high density site, and over a bare patch at the low density site. Therefore, the true densities for these hydrodynamic measurements were closer to 100 and 0%, and these sites are referred to as vegetated and unvegetated, respectively.

The 3 cm Vectrino profile was set to 4 locations above the sediment surface at the vegetated site: 0–3, 5–8, 10–13, and 18–21 cm, with only the bottom 3 locations sampled over the unvegetated site. At the vegetated site, a small patch was cleared within the algae to ensure no interference between the algae and ADV data collection. As the algal canopy was ~10 cm above the sediment surface, these 4 locations represent the sediment–water interface, halfway point between the seafloor and the top of algal canopy, top of canopy, and above canopy, respectively. During Vectrino measurements, an additional Vector point ADV continuously recording at 64 Hz was deployed on the same aluminum frame as the Vectrino (Fig. 1C) in order to determine upper water column (i.e. free stream) flow velocity and turbulence conditions. The measurement volume of this Vector was set to 35 cm above the sediment surface. Three complete velocity profiles were made at each site, with each profile consisting of the 3 or 4 locations sampled in succession for 3 min bursts with the Vectrino measuring at 25 Hz. This averaging interval was chosen to minimize changes in mean velocity due to tidal flow, as the Vectrino had to be manually moved between each measurement height.

A 2-step coordinate rotation was performed on all velocity data collected by the Vectrino and Vector. Mean flow was assigned to the horizontal direction u, with the mean transverse velocity $\bar{v}$ and mean vertical velocity $\bar{w}$ set to 0. Following rotation, these data were spectrally decomposed to separate turbulent fluctuations from wave motions as described by Bricker & Monismith (2007). This technique uses a Fourier transform to convert velocity data from the time to the frequency domain, allowing the total energy contributed at the wave frequency in the power spectrum to be removed from the combined spectral sum.

For each Vectrino bin, and for the Vector measurements, the Reynolds stress (RS) was calculated as:

$$\overline{\text{RS}} = \overline{u'w'} \quad (5)$$

where u' and w' are the spectrally decomposed turbulent fluctuations of the rotated horizontal and vertical velocity, respectively. Rotated, decomposed values of u', v', and w' were also used to calculate the turbulent kinetic energy (TKE) for each Vectrino bin:

$$\overline{\text{TKE}} = 0.5 \times \sqrt{\overline{u'u'} + \overline{v'v'} + \overline{w'w'}} \quad (6)$$

Values of u, RS, and TKE were averaged together along each 3 cm profile. These mean values were then normalized against rotated Vector velocities taken at the 35 cm measuring height (u_{35}) for better comparison between the sites.

Bed shear stress (τ_b) was calculated at each site using the mean TKE calculated for the 0–3 cm measuring height (Hansen & Reidenbach 2013, Stocking et al. 2016):

$$\tau_b = 0.19 \times \rho \times \text{TKE}_{0-3\text{cm}} \quad (7)$$

where ρ is the density of seawater at 25°C and a salinity of 35 (1022 kg m^{-3}).

2.4. Error and statistical tests

Error estimates for R were represented as the standard error (SE) of the mean nighttime flux. Error for GPP and NEM at the high density site was represented as the propagation of hourly flux SE based on Eqs. (2) & (3), while error for u, RS, TKE, and τ_b was represented as the propagation of SE from Vector and Vectrino measurements. Propagation of error was defined as (Ku 1966):

$$SE_A = \sqrt{\left(\frac{\partial A}{\partial X} \times SE_X\right)^2 + \left(\frac{\partial A}{\partial Y} \times SE_Y\right)^2 + \cdots} \quad (8)$$

where A is a function of independent variables X and Y, i.e. $A = A(X, Y, \ldots)$, and $\frac{\partial A}{\partial X}$ and $\frac{\partial A}{\partial Y}$ represent the partial derivatives of A with respect to X and Y, respectively. Due to our daytime interpolation, we did not assign error to GPP or NEM at the low density site, and these values represent point estimates.

In addition to the P-I equation (Eq. 4), the daytime flux vs. PAR relationships at both sites were fit with linear regressions in order to test statistical significance. Flow speed vs. nighttime flux was also linearly regressed at both sites to test for significance.

Previous measurements of oxygen flux were made over this same tidal flat 2 yr prior to our study, during which time the flat was nearly devoid of algae. Mean nighttime and daytime flux between bare, low density, and high density sites were tested for statistical differences using a 1-way ANOVA.

3. RESULTS

3.1. Site characteristics

Water column oxygen concentration and horizontal flow speed (15 min averages) at the 2 sites ranged from 128–271 µmol l^{-1} and 0.6–30.4 cm s^{-1}, respectively. Grain size, organic matter content, and benthic chl *a* content were all similar between the 2 sites, while mean flow speed was slightly higher at the high density site (Table 1).

3.2. Oxygen flux

Example daytime and nighttime data from the high density site are presented in Fig. 2. These data are representative of what was collected at the 2 sites, and illustrate how we used turbulent fluctuations in the velocity and oxygen concentration to calculate the flux, as well as our ability to correlate flux to short-term drivers such as light. Daytime flux is closely coupled to light, while nighttime flux is relatively constant. For all fluxes, a negative value indicates an uptake of oxygen, while a positive value indicates a release.

Mean daytime and nighttime flux from the low and high density sites, as well as from past bare measurements, are presented in Fig. 3. Results from a 1-way ANOVA on these values showed that oxygen flux significantly differed among the 3 groups for both daytime ($F = 15.8$, $p < 0.001$) and nighttime ($F = 67.0$, $p < 0.001$) flux.

Linear regressions between PAR and daytime flux were significant ($p < 0.001$) for both low and high density sites. Likewise, hyperbolic tangential P-I curves are presented in Fig. 4, and show light to be an important short-term driver of oxygen flux. The light compensation points predicted by these P-I curves were 603 and 268 µmol photons m^{-2} s^{-1} at the low and high density sites, respectively. Daytime PAR was above these levels during 64% of the sampling period at the low density site, and 63% of the sampling period at the high density site. The P-I relationship at the low density site was used to interpolate daytime flux values in order to calculate GPP and NEM (see Section 2.2).

The linear regression between horizontal flow speed and nighttime flux was significant ($p < 0.001$) at the high density site, but not at the low density site ($p = 0.27$; Fig. 5). Only nighttime data were used for this analysis to remove the confounding impact of light on oxygen flux. The small quantity of positive fluxes presented in Fig. 5 is attributed to either sporadic measurement bias resulting from the horizontal advection of oxygen across the measurement site (Holtappels et al. 2013), which evens out when averaging across all data, or to the residual release of oxygen during early evening hours.

Composite 24 h fluxes, used to calculate GPP and NEM, are presented in Fig. 6 along with mean hourly PAR at the high density site. R and GPP were substantially greater at the high vs. low density site, while NEM at the high density site did not significantly differ from 0, indicating metabolic balance (Fig. 7).

3.3. Hydrodynamics

Hydrodynamics were considerably altered within the algal canopy. Near-bed flow and turbulence were significantly diminished at the vegetated site, both relative to values higher in the water column, and to equivalent measurement heights at the unvegetated site

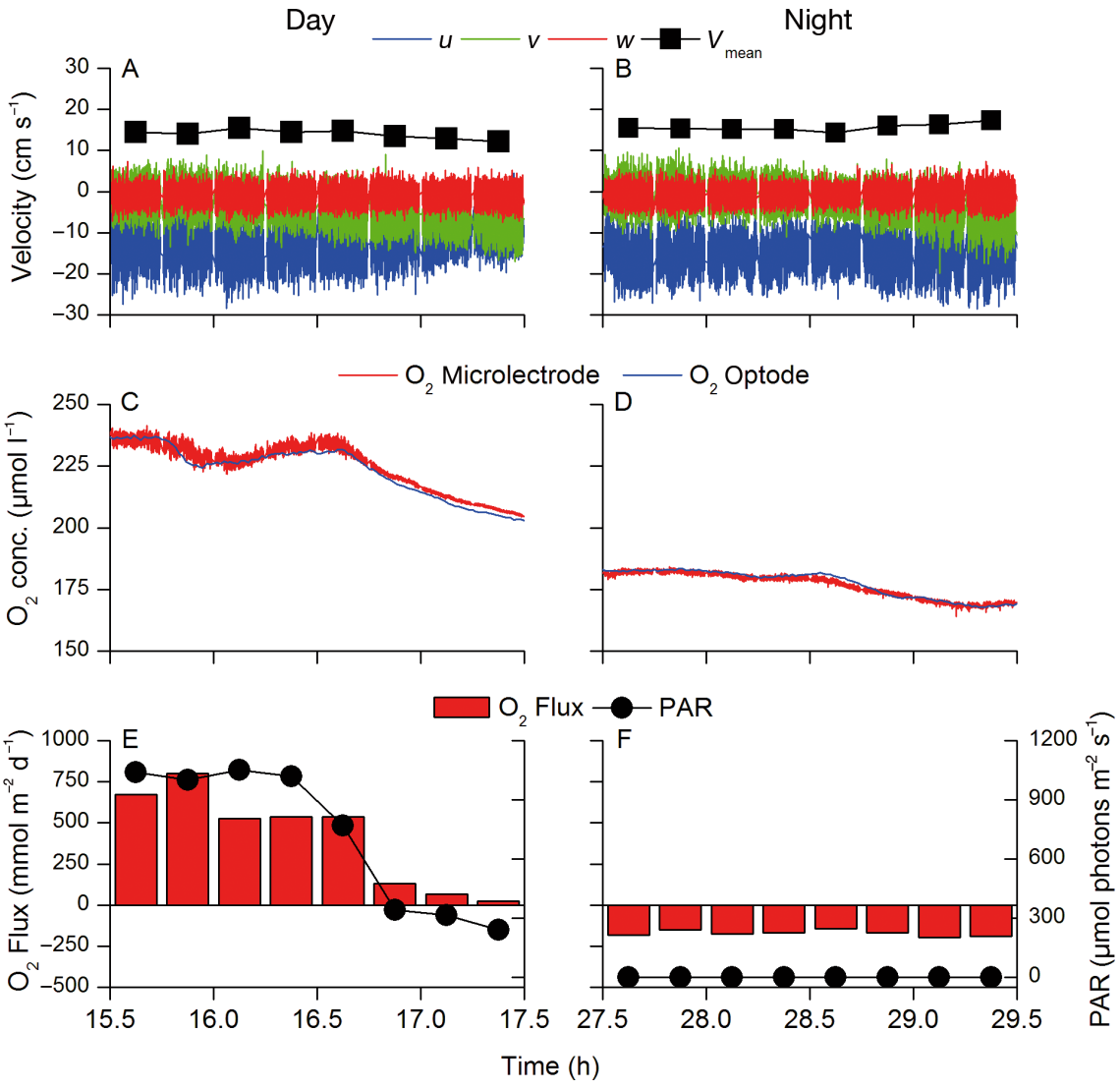

Fig. 2. Example aquatic eddy covariance data from the high density site showing (A,B) flow velocity, (C,D) dissolved oxygen concentration, and (E,F) oxygen flux and photosynthetically active radiation (PAR) during representative 2 h periods from both day and night. Vertical velocity (w) and O_2 microelectrode were used to calculate the flux (Eq. 1), while the optode was used to calibrate the microelectrode. A negative flux indicates a net uptake of oxygen, a positive flux indicates a release. Data shown were collected during the afternoon and early morning of 16–17 June 2017. Note the strong relationship between light and daytime release, while nighttime uptake is relatively constant

(Table 2). Unvegetated Vectrino data for the 5–8 cm profile were corrupted during each of the 3 trials, presumably due to the so-called 'weak spot' that can result in ADV data from sound reflectance with the seafloor. As a result, these data were discarded, and only 3 data points were used for these profiles (mean of 0–3 and 10–13 cm Vectrino profiles, and 35 cm Vector data).

When normalized by the free stream velocity measured 35 cm above the seafloor (u_{35}), horizontal flow speed (u) was significantly greater at both the 0–3 and 10–13 cm heights at the unvegetated site than at the vegetated site. Above the canopy, flow speed at the vegetated site sharply increased, and u rapidly approached free stream conditions (Fig. 8A). This lack of flow within the canopy severely limited TKE (Fig. 8B) and RS (Fig. 8C). TKE was significantly lower at the vegetated site than at the unvegetated site at depths beneath the algal canopy, but was greater at depths above the algal canopy. RS was significantly dampened within the algal canopy relative to values at the unvegetated site, and approached values of unvegetated RS higher in the water column. Bed shear stress τ_b was an order of magnitude greater at the unvegetated site than at the vegetated site, with values (mean ± SE) of 0.021 ± 0.003 and 0.002 ± 0.000 Pa, respectively.

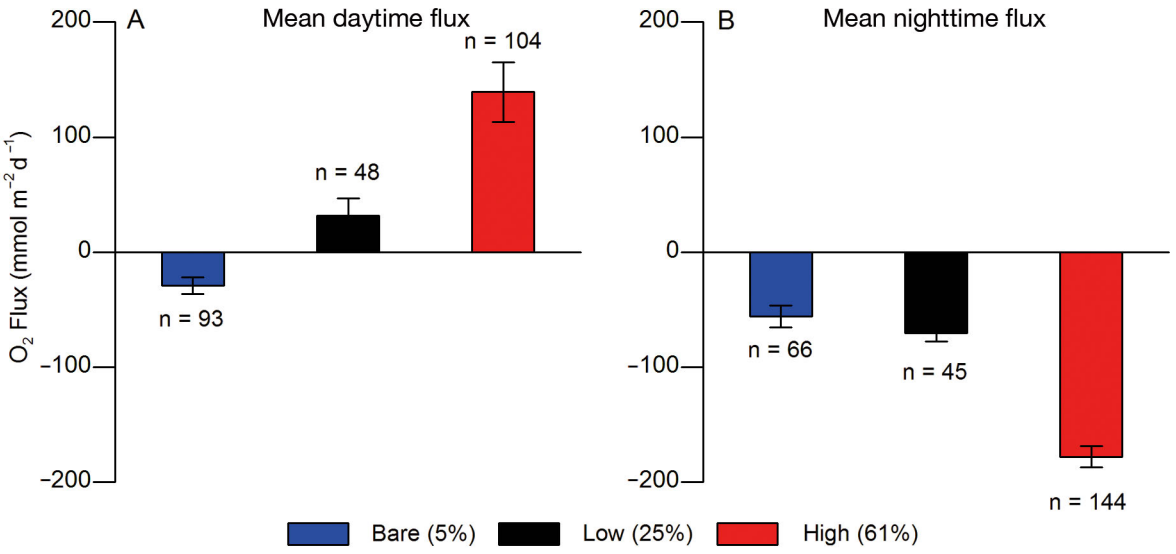

Fig. 3. Mean (A) daytime and (B) nighttime flux at the high and low density sites from our study, compared to previous values measured when this tidal flat was nearly bare, 2 yr prior to our measurements (Volaric et al. 2018). Increases in algal biomass substantially enhanced both nighttime uptake and daytime oxygen release. Flux values are ± SE, and percentages indicate algal coverage

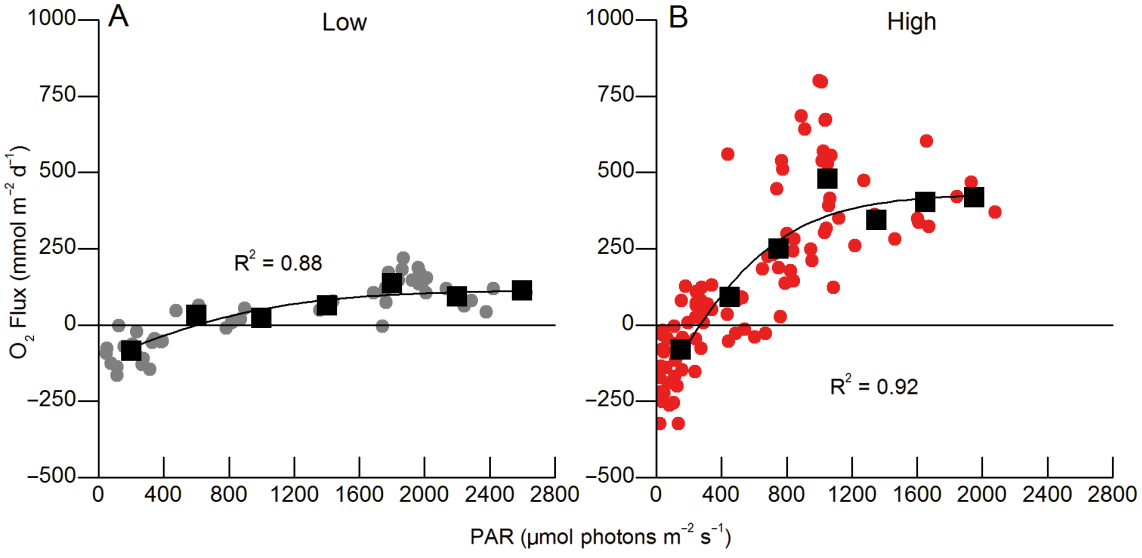

Fig. 4. Photosynthesis–irradiance (P-I) curves at (A) low density and (B) high density sites were determined as photosynthetically active radiation (PAR) vs. daytime oxygen flux. Circles: individual 15 min daytime fluxes; squares: binned data. The binned data were fit with hyperbolic tangent functions, allowing for the prediction of the light compensation point (*x*-intercept), respiration (*y*-intercept), and maximum oxygen production (horizontal asymptote). The P-I relationship in (A) was used to interpolate mean hourly daytime fluxes at the low density site

Representative power spectral densities show significant reductions in horizontal (S_{uu}) and vertical (S_{ww}) flow energy by the algal canopy at the vegetated site due to flow attenuation (Fig. 9). For this analysis, the middle bin (16th of 31 total) of the Vectrino data was plotted for data collected at the 0–3, 5–8, 10–13, and 18–21 cm measurement heights, which corresponds to elevations of 1.5, 6.5, 11.5, and 19.5 cm, respectively. Vector data were used at the 35 cm height. Total energy at the different measurement heights at the unvegetated site were all approximately equal. Likewise, there was little difference in the upper water column energy between the unvegetated and vegetated sites. At the vegetated site, energy at the 1.5 cm measurement height was considerably diminished compared to values higher in the water column. Additionally, energy at the 6.5 cm measurement height, which was approximately two-thirds between the seafloor and the top of the algal canopy, was lower than energy above the algal canopy.

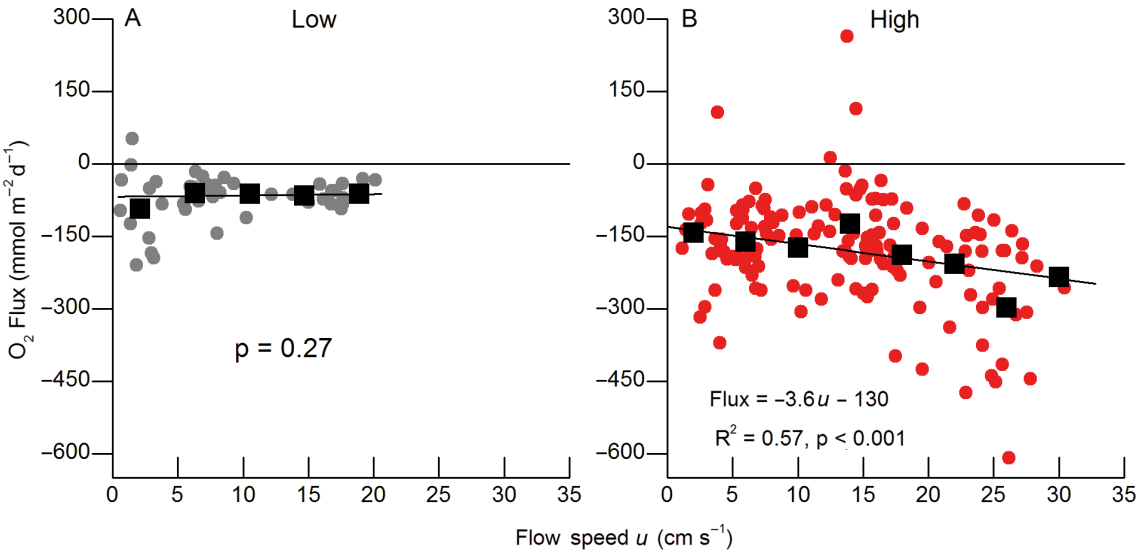

Fig. 5. Nighttime oxygen flux vs. horizontal flow speed at (A) low density and (B) high density sites. Circles: 15 min fluxes; squares; binned values. Flow speed significantly enhanced nighttime oxygen uptake over the high density site, but had no effect over the low density site. For the high density site, the best fit line and R^2 value describe binned data, while the p-values at both sites describe unbinned data

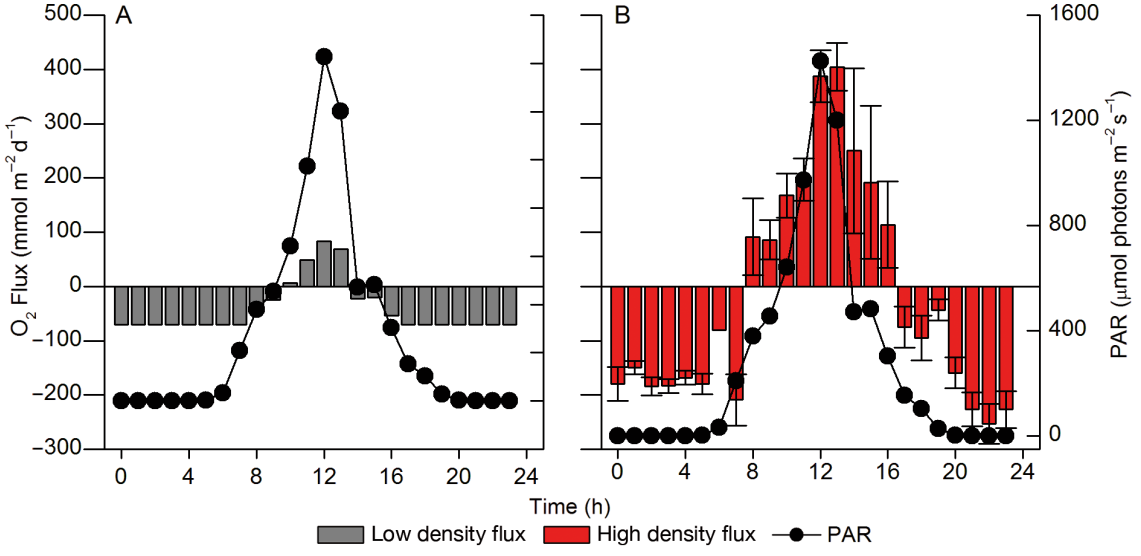

Fig. 6. Composite daily oxygen flux at (A) low density and (B) high density sites. Each column in (B) represents the mean of all 15 min values for each hour ± SE (n = 1–16). Nighttime values in (A) are the mean nighttime flux, while daytime values were interpolated using the P-I relationship in Fig. 4A with mean hourly photosynthetically active radiation (PAR) from the high density site. These composite fluxes were used to calculate gross primary production (Eq. 2) and net ecosystem metabolism (Eq. 3) for both sites

4. DISCUSSION

4.1. Oxygen metabolism of *Gracilaria* mats

Our research was conducted within the VCR, which, like much of the US east coast, has experienced a substantial *Gracilaria* invasion. Algal biomass on vegetated tidal flats now ranges from 9–40 g dry weight m^{-2}, approximately two-thirds of which is *Gracilaria* (Besterman & Pace 2018). This invasion has been particularly notable at our study site, as during 2015 AEC measurements performed 2 yr prior to our study, the flat was noted to have minimal algal coverage (Volaric et al. 2018). This previous study was also performed in June, and it had a similar length of day and water temperature (28.2°C in 2015 vs. 25.5°C in 2017). Comparing our mean light and dark fluxes with 2015 values shows significant increases in both daytime oxygen release and nighttime oxygen uptake at increasing algal densities,

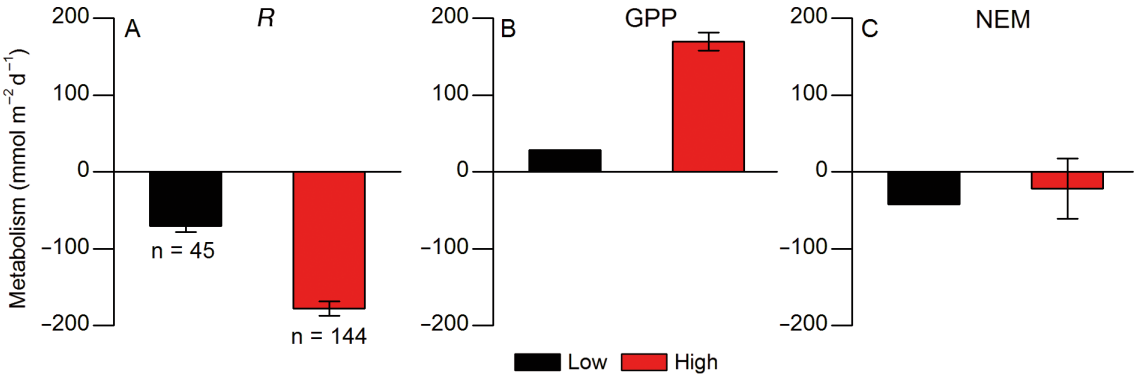

Fig. 7. Summary of oxygen metabolism values showing (A) respiration (*R*), (B) gross primary production (GPP), and (C) net ecosystem metabolism (NEM). *R* was defined as the mean nighttime flux, while GPP and NEM were calculated from the composite hourly values in Fig. 6 using Eqs. (2) & (3), respectively. Bars represent SE. Due to the interpolation of daytime values, we did not calculate an error range for GPP and NEM at the low density site

including a >300% increase in nighttime uptake from bare to dense algal coverage (Fig. 3). Additionally, both respiration (*R*), and GPP were much greater at the high vs. low density site (*R*: −178 vs. −71 mmol m^{-2} d^{-1}, GPP: 169 vs. 29 mmol m^{-2} d^{-1}; Fig. 7), indicating enhanced oxygen metabolism as the invasion has progressed.

Although our measurements were made under submerged conditions, they are likely a good first-order approximation of the true 24 h metabolism of these intertidal systems. The tidal flat in this study is submerged approximately 75% of the time, so our results describe the majority of its functioning. Additionally, our results agree with previous metabolism measurements of exposed *Gracilaria* mats by Davoult et al. (2017), who measured the emergent carbon dioxide flux using *in situ* light and dark chambers. The sediment surface enclosed within these chambers had >50% algal coverage, comparable to the mean algal coverage of our high density site (61%). Assuming a 1 to 1 photosynthetic relationship between CO_2 and O_2, they reported a mean summer *R* of −150 mmol m^{-2} d^{-1}, and a mean light flux of 240 mmol m^{-2} d^{-1} (Davoult et al. 2017). This exposed *R* was very close to our value, while the light flux fell within the range of hourly daytime fluxes recorded at the high density site (Fig. 6B). To our knowledge, there has been only 1 previous study of submerged *Gracilaria* metabolism (Cacabelos et al. 2012), in which the oxygen flux was measured *ex situ* via light and dark incubations. Those authors reported a similar *R* to our study (−190 mmol m^{-2} d^{-1}), as well as a light flux (1000 mmol m^{-2} d^{-1}) that was similar to the maximum fluxes we recorded (800 mmol m^{-2} d^{-1}; Fig. 4).

Seasonal biomass of *Gracilaria* within the VCR peaks in the early summer, when our measurements were made, and is at a minimum in the winter (Thomsen et al. 2006). Given this high biomass, as well as high light levels associated with the early summer, both GPP and *R* were likely near their seasonal maxima, a pattern that has been shown for other benthic substrates including a restored VCR *Zostera marina* seagrass meadow (Rheuban et al. 2014a). In many ways, the invasion of *Gracilaria* onto previously bare tidal

Table 2. Summary of mean hydrodynamic parameters taken by the Vectrino (measurement height = 0–21 cm) and Vector (measurement height = 35 cm). Values represent raw means ± SE. Each Vectrino profile consisted of 31 data points along a 3 cm vertical profile. As free stream flow speed (u_{35}) was greater during data collection at the unvegetated site than the vegetated site, u_{35} was used to normalize values of flow speed (u), turbulent kinetic energy (TKE), and Reynolds stress (RS) for better comparison between the 2 sites (Fig. 8). –: data not available

	Unvegetated			Vegetated		
Measurement height (cm)	u (cm s^{-1})	TKE (cm^2 s^{-2})	RS (cm^2 s^{-2})	u (cm s^{-1})	TKE (cm^2 s^{-2})	RS (cm^2 s^{-2})
0–3	5.71 ± 0.82	1.06 ± 0.04	−0.45 ± 0.08	0.14 ± 0.03	0.10 ± 0.01	−0.01 ± 0.00
5–8	–	–	–	0.45 ± 0.10	0.35 ± 0.04	−0.04 ± 0.01
10–13	7.27 ± 1.10	0.96 ± 0.07	−0.59 ± 0.11	1.20 ± 0.22	0.56 ± 0.05	−0.12 ± 0.02
18–21	–	–	–	3.25 ± 0.35	0.98 ± 0.05	−0.23 ± 0.02
35	9.40 ± 0.25	1.12 ± 0.02	−1.13 ± 0.14	6.57 ± 0.27	1.33 ± 0.04	−0.49 ± 0.06

flats represents an analogous state change to the restoration of this meadow. Initially seeded over bare subtidal sediments (Orth et al. 2006), the meadow experienced rapid increases in metabolism as it aged. Approximately 6 yr after initial seeding, summer R and GPP were −136 and 155 mmol m^{-2} d^{-1} (Hume et al. 2011), respectively, similar to values recorded over the high density *Gracilaria* site. By 10 yr after seagrass seeding, summer R and GPP had increased to −440 and 475 mmol m^{-2} d^{-1}, respectively, due to enhanced seagrass density (Rheuban et al. 2014a). The *Gracilaria* mat has likewise experienced increasing nighttime uptake and nighttime release with increasing density (Fig. 3). However, despite increased metabolism, both this seagrass meadow (Rheuban et al. 2014a) and the algal mat remained metabolically balanced, as NEM at the high density site was not significantly different from 0 (−22 ± 39 mmol m^{-2} d^{-1}; Fig. 7).

Past AEC studies have shown that light and flow speed are often important drivers of oxygen flux for phototrophic benthic ecosystems (e.g. Hume et al. 2011, Attard et al. 2015), and both of these parameters were found to be significant for the high density site (Figs. 4B & 5B). There are several ways in which flow speed impacts oxygen flux, including by decreasing the thickness of the diffusive boundary layer at the algae–water interface (Hurd 2000), which enhances diffusive transport, and by increasing sediment resuspension, which can stimulate oxygen consumption (Glud 2008, Almroth et al. 2009). Interestingly, despite the shallow nature of the tidal flat, neither site showed signs of photoinhibition, although both showed maximum oxygen production occurring around ~2500 µmol photons m^{-2} s^{-1} (Fig. 4). These data were collected in June near the summer solstice, so these light levels represent the near-maximum values these systems will experience, albeit only under submerged conditions. The lack of photoinhibition at these levels suggests that *Gracilaria* is

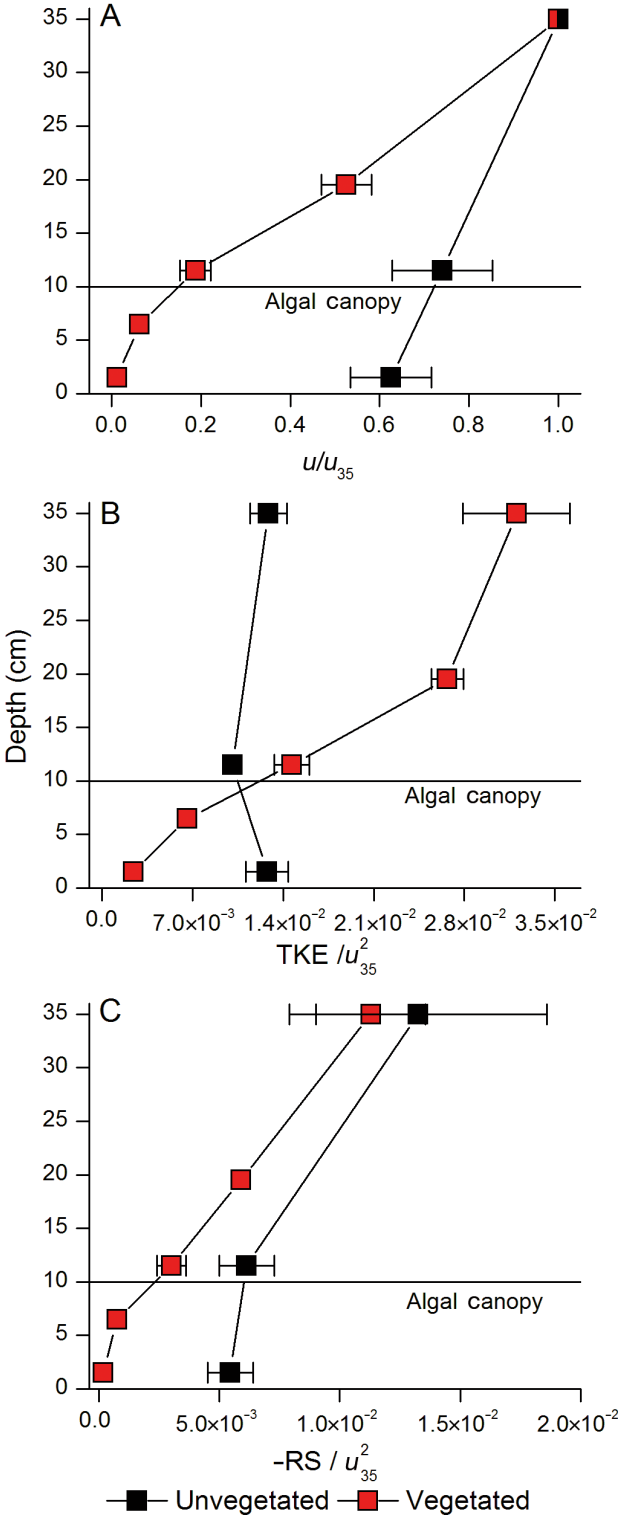

Fig. 8. Vertical profiles of (A) horizontal flow speed (u), (B) turbulent kinetic energy (TKE), and (C) Reynolds stress (RS) normalized against the free stream flow speed measured at a 35 cm measuring height (u_{35}). TKE approximates the magnitude of water column turbulence, while RS describes the downward transfer of horizontal momentum (i.e. frictional interaction with the seafloor). The presence of *Gracilaria* severely diminished flow and turbulence within the canopy, and increased turbulence intensity higher in the water column. All values below 35 cm represent averages across 31 measurements along a 3 cm vertical profile recorded using a Vectrino profiling acoustic Doppler velocimeter (ADV), while the 35 cm measurement was taken by a Vector point ADV. The Vectrino was moved up and down to record these profiles with the Vector kept fixed at 35 cm. Velocities measured by the Vector at the 35 cm measuring height ranged from 8–11 cm s^{-1} at unvegetated site, and 5–9 cm s^{-1} at the vegetated site. The averaging interval for all measurements was 3 min. Bars represent SE. Absence of bars indicates error less than symbol width as plotted

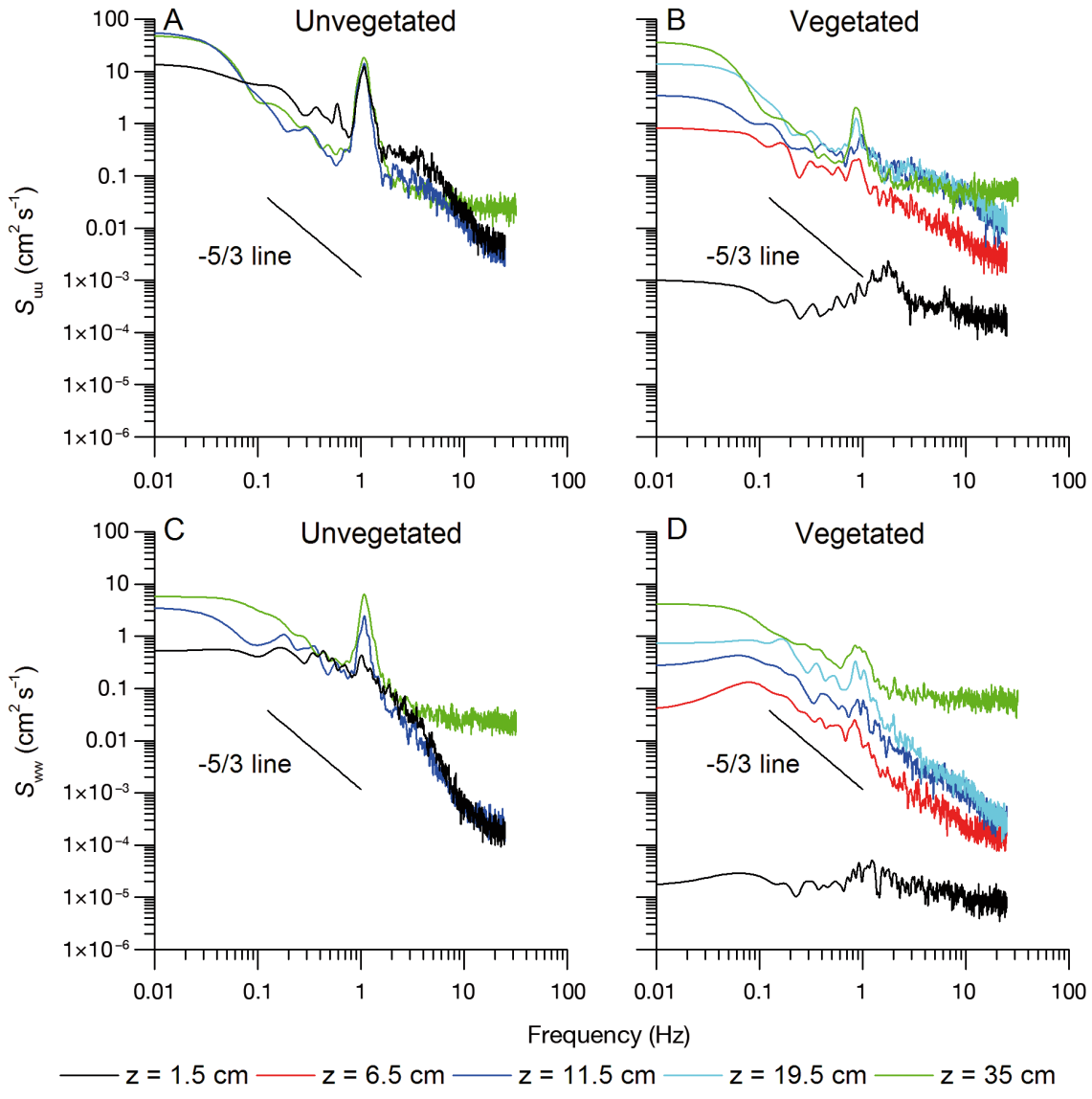

Fig. 9. Power spectral density (PSD) for (A,B) horizontal energy S_{uu} and (C,D) vertical energy S_{ww} across a range of frequencies for different measurement heights above unvegetated and vegetated sites. All data except at the 35 cm measurement height were taken from the 16th of 31 bins across a 3 cm Vectrino profile. The 35 cm data were collected using a Vector. The canopy height of the *Gracilaria* mat was 10 cm. Total energy increased with distance from the seafloor at the vegetated site, but was relatively constant at the unvegetated site, showing the impact of *Gracilaria* on flow attenuation. The spectral peaks around ~1 Hz are due to wave orbitals, while PSDs at higher frequencies are expected to follow a characteristic −5/3 slope indicative of the rate of turbulence dissipation. The deviation from this −5/3 line at higher frequencies for data at the 35 cm measuring height is attributed to the higher noise floor of the Vector relative to the Vectrino

well adapted to the shallow intertidal zone, partially explaining its success in colonizing these previously bare tidal flats.

Past studies have shown that *Gracilaria* either has minimal (Besterman & Pace 2018) or negative (Hardison et al. 2013) impacts on benthic microalgal production. Accordingly, enhanced tidal flat metabolism is likely spurred directly by this addition of a large phototrophic biomass, rather than by changes to the microphytobenthos. Increased primary production has significant implications for native macrofauna. Although *Gracilaria* has been shown to have low palatability (Hammann et al. 2013), several macrofauna likely consume it via detrital pathways (Byers et al. 2012, Davoult et al. 2017). Therefore, this enhanced carbon fixation may account for some of the increase in macrofaunal biomass typically associated with these mats (e.g. Nyberg et al. 2009, Davoult et al. 2017, Ramus et al. 2017).

4.2. Hydrodynamics and sediment transport

Vertical profiles in horizontal flow speed (u), TKE, and RS at the vegetated site were typical for flow within and above dense aquatic vegetation, including turf algae (Larned et al. 2011, Stocking et al. 2016) and seagrass meadows (Hansen & Reidenbach 2013). All 3 parameters were considerably diminished within the algal canopy relative to the unvegetated site due to flow attenuation. Above the canopy, vegetated values of u and RS approached values recorded over the unvegetated site, while above-canopy TKE was greater (Fig. 8). These patterns are indicative of flow skimming above this dense patch of algae. Due to this skimming interaction, the presence of *Gracilaria* did not enhance the downward transfer of vertical momentum (i.e. RS) relative to bare sediments, despite higher rates of water column mixing (i.e. TKE). This relationship likely arises from the high density of the *Gracilaria* where the measurements were made, and may not occur at more intermediate densities that allow for more flow penetration (e.g. Hansen & Reidenbach 2017).

Dampening of flow energy within the algal canopy (Fig. 9) led to bed shear stress (τ_b) an order of magnitude lower at the vegetated site (0.002 Pa) vs. the unvegetated site (0.021 Pa). This diminishment of bed shear agrees with other studies involving flows surrounding dense vegetation (Finnigan 2000, Venier et al. 2012). Unvegetated site τ_b was near the critical threshold (0.04 Pa) necessary to resuspend coastal muddy sediments (Lawson et al. 2007), indicating that the presence of *Gracilaria* on tidal flats may help to stabilize sediments under these flow conditions.

Hydrodynamic measurements were made on a flood tide with a free stream velocity (u_{35}) <11 cm s^{-1} (Table 2). This flow speed is near the threshold (11–13 cm s^{-1}) at which unattached *Gracilaria* can be transported as bedload, disturbing sediments and increasing sediment resuspension (Canal-Vergés et al. 2010, Lawson et al. 2012), but far beneath that necessary to detach algae from *Diopatra cuprea* worm tubes (40–120 cm s^{-1}; Thomsen 2004). Velocity data from AEC measurements indicate that the flow speed at these sites can exceed 30 cm s^{-1} during ebb tide, and although much of the *Gracilaria* at both sites was attached to *D. cuprea* tubes, there was some quantity of unattached algae that appeared to have moved in between field days. Therefore, at higher flow speeds, *Gracilaria* may enhance resuspension by scouring sediments as it moves along the bed. These competing processes likely result in complex, flow-dependent sediment dynamics, in which deposition and resuspension are each stimulated under different flow conditions, similar to those observed in other intertidal systems such as oyster reefs (Reidenbach et al. 2013). These complex dynamics may partially explain results reported by Ramus et al. (2017), who found a negative correlation between *Gracilaria* biomass and the dissolution of gypsum blocks, indicating enhanced flow attenuation, yet recorded only a weak, non-significant effect of biomass on sediment stabilization.

Mass transfer of solutes across the sediment–water interface is directly correlated to bed shear stress (Hondzo 1998, Reidenbach et al. 2010). Certain burrowing infauna, such as polychaete worms, rely on mass transfer in order to acquire oxygen and expel waste (Kristensen 1985, Murphy & Reidenbach 2016). By inhibiting this exchange, the presence of *Gracilaria* may negatively impact such burrowing organisms, particularly those unable to consume it as a food source. Coastal sediments can also be sources of many elements, including mercury and other heavy metals (Warnken et al. 2001, Choe et al. 2004), as well as nitrogen, silica, and phosphorus (Callender & Hammond 1982). Limiting benthic exchange not only restricts the diffusive flux of these materials into the water column, it also decreases the sediment oxygen penetration depth (Cai & Sayles 1996), which can affect their cycling. For example, exposure to oxygen in the sediments has been shown to greatly enhance rates of denitrification and dissimilatory nitrate reduction to ammonia in seagrass meadows (Aoki & McGlathery 2018).

5. CONCLUSIONS

Our results supported our hypotheses, as through the addition of a large phototrophic biomass, the invasion of *Gracilaria* has enhanced the ecosystem metabolism and significantly altered the hydrodynamics of tidal flats. Both parameters are inextricably linked in submerged aquatic vegetation, given that hydrodynamics are a dominant driver of the production and resource acquisition of macroalgal beds (Hurd 2000). Therefore, by altering the local flow environment, *Gracilaria* has modified tidal flats not only for native organisms, but for itself as well. This new hydrodynamic environment is likely beneficial to *Gracilaria*, partially explaining its invasion success. Decreased flow near the surface increases retention of solutes within the mat and decreases the risk of detachment and/or advective transport off of

tidal flats (Larned et al. 2011), suggesting a positive feedback for invasive macroalgal growth and proliferation. As invasive macroalgae increase in density and areal coverage, the physical environment becomes more amenable to macroalgal function, leading to further growth, resulting in further alteration of the physical environment. This feedback implies that there may be some critical density above which invasive macroalgae rapidly proliferate within previously bare native systems, suggesting that initial management is crucial to prevent long-term establishment.

Acknowledgements. We thank B. Lusk and The Nature Conservancy for providing access to the field sites. We also thank D. Boyd and D. Martin for field assistance, L. Aoki and M. Miller for laboratory assistance, and J. Stocking, A. Besterman, and A. Berger for research guidance. Support for this study was provided by the National Science Foundation (NSF) through grants for the Virginia Coast Reserve Long-Term Ecological Research program (DEB-1237733 and DEB-1832221) and Chemical Oceanography program (OCE-1334848) to P.B. Support was also provided by the University of Virginia.

LITERATURE CITED

Almroth E, Tengberg A, Andersson JH, Pakhomova S, Hall POJ (2009) Effects of resuspension on benthic fluxes of oxygen, nutrients, dissolved inorganic carbon, iron and manganese in the Gulf of Finland, Baltic Sea. Cont Shelf Res 29:807–818

Aoki LR, McGlathery KJ (2018) Restoration enhances denitrification and DNRA in subsurface sediments of *Zostera marina* seagrass meadows. Mar Ecol Prog Ser 602:87–102

Attard KM, Stahl H, Kamenos NA, Turner G, Burdett HL, Glud RN (2015) Benthic oxygen exchange in a live coralline algal bed and an adjacent sandy habitat: an eddy covariance study. Mar Ecol Prog Ser 535:99–115

Attard KM, Rodil IF, Berg P, Norkko J, Norkko A, Glud RN (2019) Seasonal metabolism and carbon export potential of a key coastal habitat: the perennial canopy-forming macroalga *Fucus vesiculosus.* Limnol Oceanogr 64: 149–164

Berg P, Huettel M (2008) Monitoring the seafloor using the noninvasive eddy correlation technique: integrated benthic exchange dynamics. Oceanography 21:164–167

Berg P, Røy H, Janssen F, Meyer V, Jørgensen BB, Huettel M, de Beer D (2003) Oxygen uptake by aquatic sediments measured with a novel non-invasive eddy-correlation technique. Mar Ecol Prog Ser 261:75–83

Berg P, Røy H, Wiberg PL (2007) Eddy correlation flux measurements: the sediment surface area that contributes to the flux. Limnol Oceanogr 52:1672–1684

Berg P, Glud RN, Hume A, Stahl H, Oguri K, Meyer V, Kitazato H (2009) Eddy correlation measurements of oxygen uptake in deep ocean sediments. Limnol Oceanogr Methods 7:576–584

Berg P, Reimers CE, Rosman JH, Huettel M, Delgard ML, Reidenbach MA, Özkan-Haller HT (2015) Time lag correction of aquatic eddy covariance data measured in the presence of waves. Biogeosciences 12:6721–6735

Berg P, Delgard ML, Polsenaere P, McGlathery KJ, Doney SC, Berger AC (2019) Dynamics of benthic metabolism, O_2, and pCO_2 in a temperate seagrass meadow. Limnol Oceanogr (in press), https://doi.org/10.1002/lno.11236

Besterman AF, Pace ML (2018) Do macroalgal mats impact microphytobenthos on mudflats? Evidence from a meta-analysis, comparative survey, and large-scale manipulation. Estuaries Coasts 41:2304–2316

Boudreau BP, Jørgensen BB (2001) The benthic boundary layer. Oxford University Press, New York, NY

Bricker JD, Monismith SG (2007) Spectral wave-turbulence decomposition. J Atmos Ocean Technol 24:1479–1487

Byers JE, Sotka EE (2019) Promoting invasive species to enhance multifunctionality in a native ecosystem still requires strong(er) scrutiny. Biol Invasions 21:277–280

Byers JE, Gribben PE, Yeager C, Sotka EE (2012) Impacts of an abundant introduced ecosystem engineer within mudflats of the southeastern US coast. Biol Invasions 14: 2587–2600

Cacabelos E, Engelen AH, Mejia A, Arenas F (2012) Comparison of the assemblage functioning of estuary systems dominated by the seagrass *Nanozostera noltii* versus the invasive drift seaweed *Gracilaria vermiculophylla.* J Sea Res 72:99–105

Cai W, Sayles FL (1996) Oxygen penetration depths and fluxes in marine sediments. Mar Chem 52:123–131

Callender E, Hammond DE (1982) Nutrient exchange across the sediment-water interface in the Potomac River estuary. Estuar Coast Shelf Sci 15:395–413

Canal-Vergés P, Vedel M, Valdemarsen T, Kristensen E, Flindt MR (2010) Resuspension created by bedload transport of macroalgae: implications for ecosystem functioning. Hydrobiologia 649:69–76

Choe K, Gill GA, Lehman RD, Han S, Heim WA, Coale KH (2004) Sediment-water exchange of total mercury and monomethyl mercury in the San Francisco Bay-Delta. Limnol Oceanogr 49:1512–1527

Davoult D, Surget G, Stiger-Pouvreau V, Noisette F and others (2017) Multiple effects of a *Gracilaria vermiculophylla* invasion on estuarine mudflat functioning and diversity. Mar Environ Res 131:227–235

Dumay O, Fernandez C, Pergent G (2002) Primary production and vegetative cycle in *Posidonia oceanica* when in competition with the green algae *Caulerpa taxifolia* and *Caulerpa racemosa.* J Mar Biol Assoc UK 82:379–387

Finnigan J (2000) Turbulence in plant canopies. Annu Rev Fluid Mech 32:519–571

Glud RN (2008) Oxygen dynamics of marine sediments. Mar Biol Res 4:243–289

Gulbransen DJ, McGlathery KJ, Marklund M, Norris JN, Gurgel CFD (2012) *Gracilaria vermiculophylla* (Rhodophyta, Gracilariales) in the Virginia coastal bays: *cox*1 analysis reveals high genetic richness of an introduced macroalga. J Phycol 48:1278–1283

Gurgel CFD, Norris JN, Schmidt WE, Le HN, Fredericq S (2018) Systematics of the Gracilariales (Rhodophyta) including new subfamilies, tribes, subgenera, and two new genera, *Agarophyton gen. nov.* and *Crassa gen. nov.* Phytotaxa 374:1–23

Hammann M, Wang G, Rickert E, Boo SM, Weinberger F (2013) Invasion success of the seaweed *Gracilaria vermiculophylla* correlates with low palatability. Mar Ecol Prog Ser 486:93–103

Hansen JCR, Reidenbach MA (2013) Seasonal growth and

senescence of a *Zostera marina* seagrass meadow alters wave-dominated flow and sediment suspension within a coastal bay. Estuaries Coasts 36:1099–1114

Hansen JCR, Reidenbach MA (2017) Turbulent mixing and fluid transport within Florida Bay seagrass meadows. Adv Water Resour 108:205–215

Hardison AK, Canuel EA, Anderson IC, Tobias CR, Veuger B, Waters MN (2013) Microphytobenthos and benthic macroalgae determine sediment organic matter composition in shallow photic sediments. Biogeosciences 10:5571–5588

Holtappels M, Glud RN, Donis D, Liu B, Hume A, Wenzhöfer F, Kuypers MMM (2013) Effects of transient bottom water currents and oxygen concentrations on benthic exchange rates as assessed by eddy correlation measurements. J Geophys Res Oceans 118:1157–1169

Hondzo M (1998) Dissolved oxygen transfer at the sediment-water interface in a turbulent flow. Water Resour Res 34: 3525–3533

Hume A, Berg P, McGlathery KJ (2011) Dissolved oxygen fluxes and ecosystem metabolism in an eelgrass (*Zostera marina*) meadow measured with the eddy correlation technique. Limnol Oceanogr 56:86–96

Hurd CL (2000) Water motion, marine macroalgal physiology, and production. J Phycol 36:453–472

Inderjit, Chapman D, Ranelletti M, Kaushik S (2006) Invasive marine algae: an ecological perspective. Bot Rev 72: 153–178

Jassby AD, Platt T (1976) Mathematical formulation of the relationship between photosynthesis and light for phytoplankton. Limnol Oceanogr 21:540–547

Kristensen E (1985) Oxygen and inorganic nitrogen exchange in a *Nereis virens* (Polychaeta) bioturbated sediment-water system. J Coast Res 1:109–116

Krueger-Hadfield SA, Kollars NM, Strand AE, Byers JE and others (2017) Genetic identification and likely vector of a widespread marine invader. Ecol Evol 7:4432–4447

Krueger-Hadfield SA, Stephens TA, Ryan WH, Heiser S (2018) Everywhere you look, everywhere you go, there's an estuary invaded by the red seaweed *Gracilaria vermiculophylla* (Ohmi) Papenfuss, 1967. BioInvasions Rec 7:343–355

Ku HH (1966) Notes on the use of propagation of error formulas. J Res Natl Bur Stand 70:263–273

Larned ST, Packman AI, Plew DR, Vopel K (2011) Interactions between the mat-forming alga *Didymosphenia geminata* and its hydrodynamic environment. Limnol Oceanogr Fluids Environ 1:4–22

Lawson SE, Wiberg PL, McGlathery KJ, Fugate DC (2007) Wind-driven sediment suspension controls light availability in a shallow coastal lagoon. Estuaries Coasts 30: 102–122

Lawson SE, McGlathery KJ, Wiberg PL (2012) Enhancement of sediment suspension and nutrient flux by benthic macrophytes at low biomass. Mar Ecol Prog Ser 448: 259–270

Lee X, Massman W, Law B (2004) Handbook of micrometeorology: a guide for surface flux measurement and analysis. Kluwer Academic Publishers, Dordrecht

Long MH, Rheuban JE, Berg P, Zieman JC (2012) A comparison and correction of light intensity loggers to photosynthetically active radiation sensors. Limnol Oceanogr Methods 10:416–424

Lorenzen CJ (1967) Determination of chlorophyll and pheopigments: spectrophotometric equations. Limnol Oceanogr 12:343–346

Lorrai L, McGinnis DF, Berg P, Brand A, Wüest A (2010) Application of oxygen eddy correlation in aquatic systems. J Am Meteorol Soc 27:1533–1545

Lyons DA, Arvanitidis C, Blight AJ, Chatzinikolaou E and others (2014) Macroalgal blooms alter community structure and primary productivity in marine ecosystems. Glob Change Biol 20:2712–2724

Murphy EAK, Reidenbach MA (2016) Oxygen transport in periodically ventilated polychaete burrows. Mar Biol 163:208

Nyberg CD, Thomsen MS, Wallentinus I (2009) Flora and fauna associated with the introduced red alga *Gracilaria vermiculophylla*. Eur J Phycol 44:395–403

Ohmi H (1956) Contributions to the knowledge of Gracilariaceae from Japan. II. On a new species of the genus *Gracilariopsis*, with some considerations on its ecology. Bull Fac Fish Hokkaido Univ 6:271–279

Orth RJ, Luckenbach ML, Marion SR, Moore KA, Wilcox DJ (2006) Seagrass recovery in the Delmarva Coastal Bays, USA. Aquat Bot 84:26–36

Priestly CHB, Swinbank WC (1947) Vertical transport of heat by turbulence in the atmosphere. Proc R Soc A 189: 543–561

Ramus AP, Silliman BR, Thomsen MS, Long ZT (2017) An invasive foundation species enhances multifunctionality in a coastal ecosystem. Proc Natl Acad Sci USA 114: 8580–8585

Reidenbach MA, Limm M, Hondzo M, Stacey MT (2010) The effects of bed roughness on boundary layer mixing and mass flux across the sediment-water interface. Water Resour Res 46:W07530

Reidenbach MA, Berg P, Hume A, Hansen JCR, Whitman ER (2013) Hydrodynamics of intertidal oyster reefs: the influence of boundary layer flow processes on sediment and oxygen exchange. Limnol Oceanogr Fluids Environ 3:225–239

Reimers CE, Özkan-Haller HT, Albright AT (2016) Microelectrode velocity effects and aquatic eddy covariance measurements under waves. J Atmos Ocean Technol 33: 263–282

Rheuban JE, Berg P (2013) The effects of spatial and temporal variability at the sediment surface on aquatic eddy correlation flux measurements. Limnol Oceanogr Methods 11:351–359

Rheuban JE, Berg P, McGlathery KJ (2014a) Multiple timescale processes drive ecosystem metabolism in eelgrass (*Zostera marina*) meadows. Mar Ecol Prog Ser 507:1–13

Rheuban JE, Berg P, McGlathery KJ (2014b) Ecosystem metabolism along a colonization gradient of eelgrass (*Zostera marina*) measured by eddy correlation. Limnol Oceanogr 59:1376–1387

Salvaterra T, Green DS, Crowe TP, O'Gorman EJ (2013) Impacts of the invasive alga *Sargassum muticum* on ecosystem functioning and food web structure. Biol Invasions 15:2563–2576

Schaffelke B, Smith JE, Hewitt CL (2006) Introduced macroalgae — a growing concern. J Appl Phycol 18:529–541

Sotka EE, Byers JE (2019) Not so fast: promoting invasive species to enhance multifunctionality in a native system requires strong(er) scrutiny. Biol Invasions 21:19–25

Stocking JB, Rippe JP, Reidenbach MA (2016) Structure and dynamics of turbulent boundary layer flow over healthy and algae-covered corals. Coral Reefs 35: 1047–1059

Thomsen MS (2004) Species, thallus size and substrate

determine macroalgal break force and break location in a low-energy soft-bottom lagoon. Aquat Bot 80:153–161

Thomsen MS, McGlathery KJ (2006) Effects of accumulations of sediments and drift algae on recruitment of sessile organisms associated with oyster reefs. J Exp Mar Biol Ecol 328:22–34

Thomsen MS, McGlathery KJ, Tyler AC (2006) Macroalgal distribution patterns in a shallow, soft-bottom lagoon, with emphasis on the nonnative *Gracilaria vermiculophylla* and *Codium fragile.* Estuaries Coasts 29:465–473

Thomsen MS, Gurgel CFD, Fredericq S, McGlathery KJ (2005) *Gracilaria vermiculophylla* (Rhodophyta, Gracilariales) in Hog Island Bay, Virginia: a cryptic alien and invasive macroalga and taxonomic correction. J Phycol 42:139–141

Thomsen MS, Ramus AP, Long ZT, Silliman BR (2019) A seaweed increases ecosystem multifunctionality when invading bare mudflats. Biol Invasions 21:27–36

Thresher RE, Kuris AM (2004) Options for managing invasive marine species. Biol Invasions 6:295–300

Tyler AC, McGlathery KJ (2006) Uptake and release of nitrogen by the macroalgae *Gracilaria vermiculophylla* (Rhodophyta). J Phycol 42:515–525

Valiela I, McClelland J, Hauxwell J, Behr PJ, Hersh D, Foreman K (1997) Macroalgal blooms in shallow estuaries: controls and ecophysiological and ecosystem consequences. Limnol Oceanogr 42:1105–1118

Venier C, Figueiredo da Silva J, McLelland SJ, Duck RW, Lanzoni S (2012) Experimental investigation of the impact of macroalgal mats on flow dynamics and sediment stability in shallow tidal areas. Estuar Coast Shelf Sci 112:52–60

Volaric MP, Berg P, Reidenbach MA (2018) Oxygen metabolism of intertidal oyster reefs measured by aquatic eddy covariance. Mar Ecol Prog Ser 599:75–91

Warnken KW, Gill GA, Griffin LL, Santschi PH (2001) Sediment-water exchange of Mn, Fe, Ni and Zn in Galveston Bay, Texas. Mar Chem 73:215–231

Editorial responsibility: Just Cebrian, Stennis Space Center, Mississippi, USA

Submitted: May 21, 2019; Accepted: September 24, 2019
Proofs received from author(s): October 6, 2019